



**HAL**  
open science

## Dielectric characterisation of rock aggregates with different grain size distributions

Benhui Fan, Frédéric Bosc, Benjamin Smaniotto, Zhong-Sen Li, Jinbo Bai,  
Cyrille Fauchard

► **To cite this version:**

Benhui Fan, Frédéric Bosc, Benjamin Smaniotto, Zhong-Sen Li, Jinbo Bai, et al.. Dielectric characterisation of rock aggregates with different grain size distributions. Road Materials and Pavement Design, 2023, pp.1-14. 10.1080/14680629.2023.2224452 . hal-04136071

**HAL Id: hal-04136071**

**<https://hal.science/hal-04136071>**

Submitted on 21 Jun 2023

**HAL** is a multi-disciplinary open access archive for the deposit and dissemination of scientific research documents, whether they are published or not. The documents may come from teaching and research institutions in France or abroad, or from public or private research centers.

L'archive ouverte pluridisciplinaire **HAL**, est destinée au dépôt et à la diffusion de documents scientifiques de niveau recherche, publiés ou non, émanant des établissements d'enseignement et de recherche français ou étrangers, des laboratoires publics ou privés.

## Dielectric Characterization of Rock Aggregates with Different Grain Size Distributions

Benhui Fan<sup>1\*</sup>, Frédéric Bosc<sup>1</sup>, Benjamin Smaniotto<sup>2</sup>, Zhong-Sen Li<sup>3</sup>, Jinbo Bai<sup>2</sup>, Cyrille Fauchard<sup>4\*</sup>

<sup>1</sup>Cerema, Research Team ENDSUM, 23 avenue Amiral Chauvin, 49136, Les Ponts de Cé, France

<sup>2</sup>Université Paris-Saclay, CentraleSupélec, ENS Paris-Saclay, CNRS, LMPS - Laboratoire de Mécanique Paris-Saclay, UMR 9026, 91190, Gif-sur-Yvette, France.

<sup>3</sup>Department of Civil Engineering, Aalto University, Espoo, 02150, Finland

<sup>4</sup>Cerema, Research Team ENDSUM, 10 chemin de la poudrière, 76120, Le Grand-Quevilly, France

benhui.fan@cerema.fr

cyrille.fauchard@cerema.fr

### Abstract

Aggregates largely influence a road's dielectric properties, which is an important physical parameter when using non-destructive methods such as ground penetrating radar to evaluate a road's geometry. Due to the irregular shapes, the direct measurement of an aggregate piece by piece in the microwave domain is not easy. To address this problem, an epoxy-based composite is used to estimate the dielectric constant of the aggregates by resonant test and mixing law calculation. As a water-free binder, the epoxy composite eliminates the water effect on the dielectric properties. Meanwhile, the distribution of each component can be studied by X-ray computed tomography, which allows knowing the composite's morphology. Moreover, the composite has a smooth surface that avoids the texture effects on the dielectric measurement. In addition, the impedance analysis of individual aggregates at low frequencies was used to evaluate the results obtained with composites and mixing laws.

### Keywords:

aggregates, dielectric permittivity, analytical approaches for dielectric mixtures, X-ray computed tomography

## Introduction

Thickness evaluation of a multilayer asphalt road is important in regular controls, which can reflect the durability and serviceability of the roads. Taking out core samples is a direct way to verify the thickness of each layer, but this way is hard to achieve continuous control along the whole road. As a highly efficient and non-destructive tool, ground penetrating radar (GPR) can be used for the thickness estimation of different layers in the roads and other structural properties like compactness, bonding, defaults, etc. (AL-Qadi and Lahouar 2005, Benedetto et al. 2016, Lai. et al. 2017). In general, GPR operates in the time domain. It is based on the emission and reception of short-duration pulses (of the order of 1 ns) and its Fast Fourier Transform is typically in the microwave frequency range, i.e., from 0.3 to 3 GHz (Robert et al. 1998, Derobert et al. 2001, Araujo et al. 2017). By testing the travel time of electromagnetic (EM) waves emitted and accepted, the thicknesses of different layers can be estimated with the knowledge of EM wave's speed. EM wave's speed is calculated by the constitutive EM properties of road materials, i.e., conductivity, dielectric permittivity, and magnetic permeability (Chen et al. 2004, Smith et al. 2021). Since road constituents are usually considered diamagnetic materials with low conductivity, especially under dry conditions, the dielectric constant of road material is a dominant parameter to analyze GPR.

Direct measuring the dielectric constant of a road material by microwave dielectric characterization is difficult since exact characterizations such as coaxial transmission/reflection cells have rigid dimensional requirements for the samples due to the limits of the device under test (DUT) (Adous et al. 2006, Wagner et al. 2013). Moreover, the exact microwave dielectric characterization is hard to be representative for the whole road if the values are just obtained from several core samples. Hence, a common way to estimate a road's dielectric constant is to apply the mixing laws based on the volumetric fractions and dielectric constants of air, bitumen, and aggregates (Looyenga 1965, Sihvola and Kong 1988). The dielectric constants of air and bitumen are well-known parameters, but the dielectric constant of aggregates is not easy to obtain, because it is almost impossible to test a large number of aggregates with heterogeneous structures piece by piece.

Some methods such as the dielectric estimation by aggregate's main mineralogy or volumetric density may provide a global reference (Ulaby. et al 1990, Dobson et al 1985, Robinson and Friedman 2003), but they are not very precise. Another conventional way is to test a certain volume of aggregates by a dielectric resonant cavity. Concretely, the aggregates are filled into a Teflon (PTFE) ring to maintain the required shape according to the size requirement of the cavity. The sample is viewed as a mixture of aggregates and air. By testing the S-parameters (reflection/transmission characteristics) and the shifting resonant frequency between the cavity with and without the sample, the dielectric constant of the sample can be calculated (Chen et al. 2004, Fauchard et al. 2013). Since the volumetric fraction of the aggregates in the mold can be calculated, then the dielectric constant of the aggregates can be further derived by analytical approaches for dielectric mixtures based on mean-field theory. The advantage of this method is its easy manipulation, but the results are usually influenced by the texture of the aggregates which decreases the effective contact between the aggregates and the metal plate in the cavity. In addition, the difference between the volumetric fractions of air in the PTFE ring is large (around 20%), which challenges the hypothesis of a diluted system when applying the analytical approaches (Asami 2002, Tuncer et al. 2012).

To address this issue, the current work presents a novel epoxy-based composite method to test the dielectric constant of aggregates. Blended with epoxy, the sample can have a smooth surface that effectively avoids contact problems. Moreover, filling the voids of aggregates with epoxy will largely reduce the air percentage in

the composite from ~20% to ~2%, which makes the composite a diluted system. Compared with other binders used in construction materials, epoxy has high processability and can easily adhere to aggregates and well wet the surface of aggregates. Meanwhile, the volumetric fraction of each component (epoxy, aggregates, and air) in the composite can be controlled during the preparation. The distribution of each component in the composite can also be determined by X-ray computed tomography (CT) (Saba et al. 2014, Li and Tang. 2019). Additionally, unlike bitumen, after curing, the mechanical properties of epoxy are quite stable at room temperature, which ensures that the composite does not undergo creeping or deformation due to environmental influences. Unlike cement, the preparation of the epoxy-based composite is water-free, which eliminates the water effect on the dielectric measurement.

To evaluate the dielectric constant of aggregates derived from epoxy composites, the dielectric constants of ten pieces of aggregates were tested by an impedance analyzer at a low-frequency range. The reason to choose the impedance analyzer is associated with the sample's preparation. As mentioned before, due to the limit of DUT (Ayoub 2018), the direct measurement of a piece of aggregate by the coaxial waveguide method (7mm outer diameter and 3.5 mm inner diameter) in the microwave domain is difficult. However, the sample for the low-frequency dielectric test is much easier to prepare, i.e., a disc with 10 mm diameter and 1 mm thickness. As the dielectric permittivity is frequency-dependent, the time-frequency relaxation model can be used to translate the dielectric constant from low frequency to high frequency (Kaatze 2013). Afterward, the dielectric permittivity of the aggregates derived from the relaxation model can be used as a reference to evaluate the dielectric constant calculated by epoxy composite.

In summary, in this study we will use three methods to characterize the dielectric constant of aggregates with different size distributions: Method 1 measures the dielectric constant of aggregates piece by piece at low frequency and then fits it at high frequency. Method 2 measures and calculates the dielectric constant of aggregates in a conventional way (PTFE ring). Method 3 measures and calculates the dielectric constant of the aggregates by epoxy-based composites. We will analyze and discuss the dielectric constant of aggregates obtained by the three methods based on the time-frequency relaxation model and different analytical approaches. It should be mentioned that, as consolidated materials, bulk rocks are not single crystals, or even polycrystals, but are the assembly of multiple materials with different symmetry properties (Ulrich 2002). Road aggregates are cut from bulk rocks with different grain sizes and textures, making them even heterogeneous. Therefore, in this study, we do not expect to be able to study a specific sample with precise microstructural characterization at the analytical level. Our aim is to develop a method that can be adaptable to microwave measurement of aggregates and provide a dielectric reference.

### **Materials and Characterizations**

The rock aggregates with different grain sizes were provided by the AGIR-CTCV quarry, Pays de la Loire, France. The components were the mixture of rhyolite and gneiss. Rhyolite is an igneous rock with a dielectric constant ranging from 4.8 to 5.7. Gneiss is a metamorphic rock whose dielectric constant is from 4.9 to 5.5 (Araujo 2017, Zheng et al. 2020). The grain size distributions of the aggregates used in the study were as follows: 6-10 mm (marked as LA, large aggregates), 4-6 mm (marked as MA, medium aggregates), and 2-4 mm (marked as SA, small aggregates), respectively. Before the experiment, the aggregates were dried in an oven at 110 °C for more than 24h. The volumetric density of the aggregates was measured with a pycnometer (ASTM D1217-20). The average results are listed in **Table 1**.

**Table 1** Volumetric densities of the aggregates with three size distributions

	LA (6-10 mm)	MA (4-6 mm)	SA (2-4 mm)
Volumetric density (kg/m <sup>3</sup> )	2.712 ± 0.004	2.701 ± 0.002	2.697 ± 0.001

To prepare the composite, the aggregates were mixed with epoxy (resin (1080S) and its curing agent (1084), purchased from Resoltech Ltd., France). The preparation of the composites was as follows: firstly, the aggregates were filled into a mold with a diameter of 50 mm and a height of 25 mm. The resin and the curing agent (100/33 weight ratio) were stirred for 5 min and then poured into the mold until fully covering the aggregates, without further compacting by the force. Afterward, the sample was left in a vacuum chamber for 30 min to reduce the air bubbles (Fan B. and Bai J. et al 2017). Finally, the epoxy curing process was performed at 60°C for 15 h. Depending on the size of the aggregates, the three composites were named Comp\_LA, Comp\_MA, and Comp\_SA. A cylindrical sample with the same dimensions was also prepared to measure the dielectric constant of pure epoxy.

X-ray computed tomography (CT) was carried out using an X50-CT scanner (North Star Imaging, USA) to characterize the morphologies of the three composites. The X-ray tube equipped with a W target was set to 200 kV with a current of 360  $\mu$ A, resulting in a power of 72 W. A copper filter with a thickness of 0.3 mm was used to limit beam hardening. The volumes of the specimen were reconstructed using 1,200 radiographs that were evenly taken when the sample rotated 360°. Each radiograph was obtained as an average of 30 frames to reduce acquisition noise. The reconstructed 3D volumes consisted of 1000  $\times$  1000  $\times$  1000 voxels, with a resolution of  $\approx$  48  $\mu$ m per voxel. The micrometer-scaled resolution of CT can provide the porosity and the adhesion between epoxy and aggregates in the composite precisely. The contents in air, epoxy, and aggregates were segmented based on their grayscale threshold along a vertical axis by a Python script.

Three methods were used to study the dielectric properties in different frequency ranges. The samples used in these methods are presented in **Figure 1**.

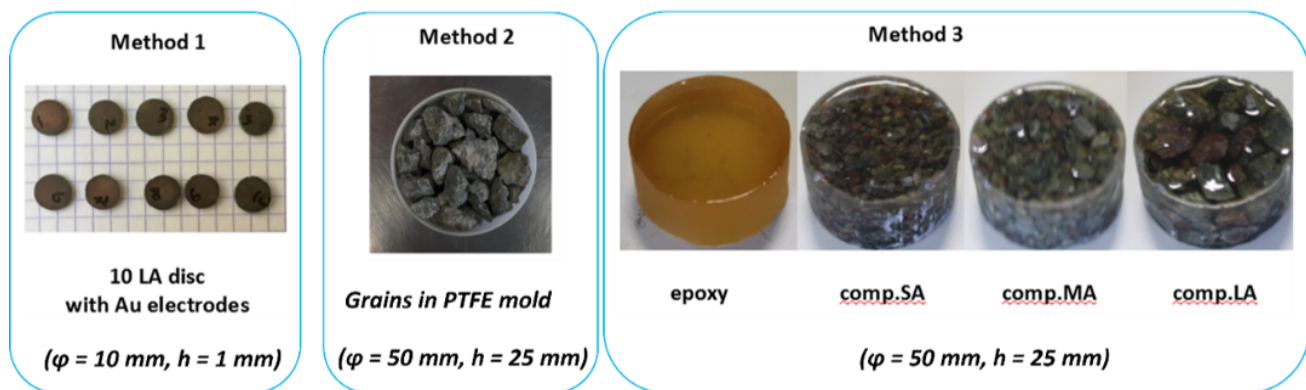


**Figure 1** Samples for the three dielectric measurements (LA, large aggregates (6-10 mm), MA, medium aggregates (4-6 mm), and SA, small aggregates (2-4 mm))

Method 1 (low-frequency impedance analysis): Limited by the minimum diameter of the electrode (10 mm) in the Solartron instrument, only aggregates with 10 mm diameters could be measured by this method in this

study. 10 pieces of LA were polished into a disc shape (with a diameter of 10 mm and a thickness of 1 mm) and tested in a wide frequency range from 1 Hz to 1 MHz by an impedance analyzer (Solartron ModuLab XM). Before the dielectric measurement, the two faces of each disc were coated with gold to reduce contact resistance. The tested disc was considered a plane capacitor and the dielectric constant was derived from the measured volumetric capacitance (Solartron analytical user guide, Andrade et al. 1999).

Method 2 (conventional method for aggregates in a PTFE ring by resonant cavity): To hold the aggregates with a cylindrical shape, the aggregates with calculated weight were put into a PTFE ring (a diameter of 50 mm, a height of 25 mm, and a thickness of 1 mm). To help the filling, a light vibration was conducted by hand, but without further compacting by other tools. The sample was placed at the center of the cavity and sandwiched between two conductive plates. The measurement of the aggregates was repeated several times to obtain the average value. The dielectric constant of the aggregates was calculated by mixing laws based on the measured dielectric constant of the aggregates/air in the PTFE ring and their volumetric fractions in **Table 2**.

**Table 2** Volumetric fractions of aggregates and air in the PTFE ring

	LA	MA	SA
Air %	28.4	25.2	22.3
Aggregates %	71.6	74.8	77.7

Method 3 (epoxy composites proposed in this work by resonant cavity): The tested composite was placed at the center of the cavity for the measurement. The dielectric constant of the aggregates was calculated by mixing laws based on the measured dielectric constant of the composite and the volumetric fractions of the aggregates, air, and epoxy in **Table 3**.

**Table 3** Volumetric fractions of aggregates, epoxy, and air in the three composites

	Air %	Epoxy %	Aggregates %
Comp_LA	2.8	49.5	47.7
Comp_MA	2.3	52.0	45.7
Comp_SA	2.8	51.8	45.4

The transmission resonant cavity (diameter of 400 mm) used in methods 2 and 3 is presented in **Figure 2 (a)**. The cavity was connected to a portable network analyzer (Agilent E8362B). The  $S_{12}$  parameter of the cavity was measured with and without a sample. The resonant frequency and its shift selected on  $S_{12}$  allow the calculation of the dielectric constant as illustrated in **Figure 2 (b)**. In the study, the resonance frequency of the samples was 540 MHz. The details of the calculation and measurement can be found in Fauchard et al. 2013.

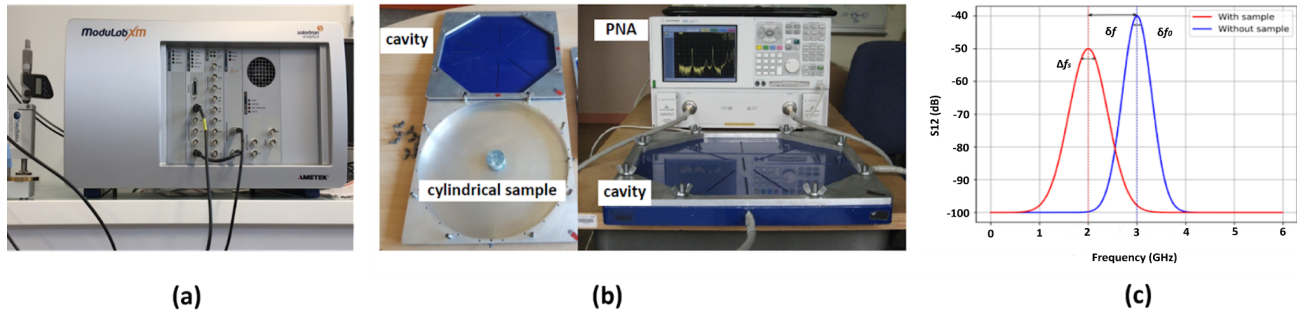


**Figure 2 (a)** Impedance analyzer. **(b)** Portable Network Analyzer showing  $S_{12}$  parameter and 400 mm cavity under test. **(c)** Resonant mode with (red curve) and without (blue curve) sample. Q factors are determined as  $Q_{L0} = f_0/\Delta f_0$  and  $Q_{Ls} = f_s/\Delta f_s$ . The bandwidths  $\delta f_0$  and  $\delta f_s$  are calculated at -3 dB compared to the max peak of resonance.

### Morphology based on X-ray computed tomography

Based on the difference in densities, the morphology of aggregates, epoxy, and air can be distinguished by computed tomography (CT) [16, 17]. As presented in **Figure 3 (a)**, first, it can be found that the aggregates have a dense structure without obvious porosity. The white points in the aggregate phase show the variety of densities in a piece of aggregate, which demonstrates its mesoscopic inhomogeneity. This inhomogeneity should be related to the various compositions caused by rock metamorphic processes and complex recrystallization processes from pre-existing formations. Moreover, it can be found that epoxy can adhere well to the aggregates and there are no obvious defects in the composites. By determining the grayscale of each component by CV2-Python package as illustrated on the right of **Figure 3 (a)**, the air, epoxy, and aggregates phases can be classified. One CT slice in the middle of each composite is taken as an example: it can be found that the blue area of air, epoxy, and aggregate in the three images can well correspond to the gray slice as presented in **Figures 3 (b), (c), and (d)**. By analyzing 355 slices in the vertical direction of each composite, the volumetric fractions of air, epoxy, and aggregates as well as their distributions from the bottom to the top of the samples can be obtained by a python script. The results are presented in **Figure 4**.

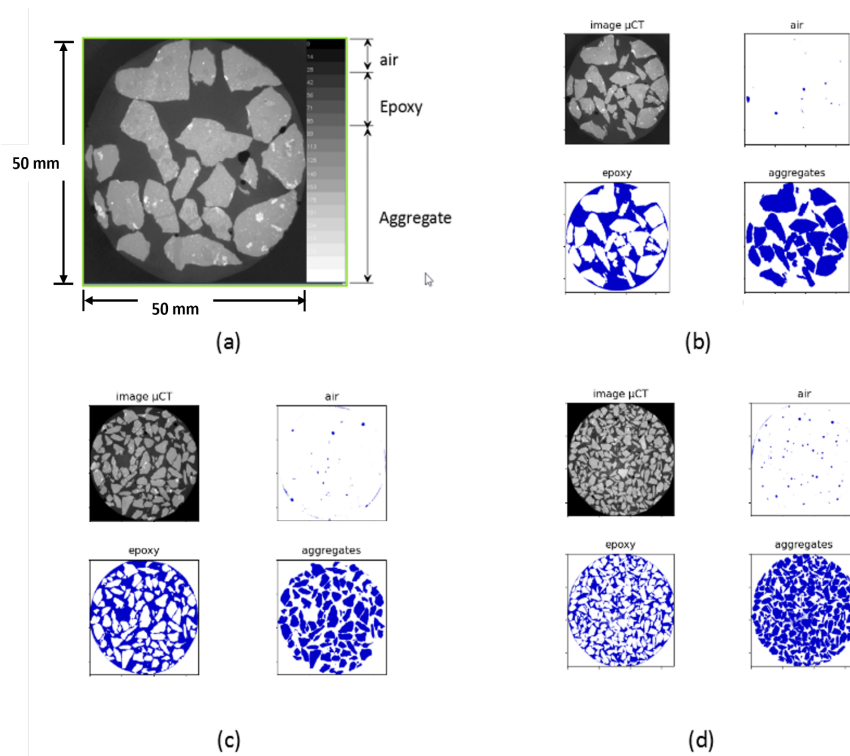


**Figure 3** (a) Analysis of the morphology by determining the threshold of grayscale of air, epoxy, and aggregates in a  $\mu$ CT slice of Comp\_LA.; (b), (c), and (d) The distributions of air, epoxy, and aggregates in a slice of Comp\_LA, Comp\_MA and Comp\_SA, respectively

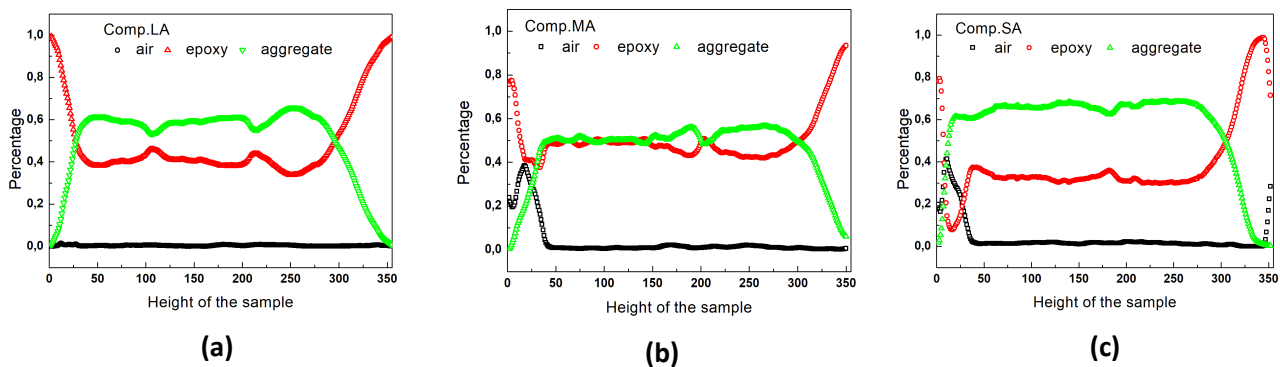


**Figure 4** Distribution of air, epoxy, and aggregates in the three composites: (a), (b) and (c) for Comp\_LA, Comp\_MA and Comp\_SA, respectively

Comparing the morphologies of the three composites, it can be found that, as the size of the grains decreases, the adherence between aggregates and epoxy decreases, and more small air bubbles appear in the interfacial regions. Meanwhile, as indicated in **Figure 4**, the distribution of air in the three composites is a bit different, though the global volumetric fraction of air in the three composites is similar (around 2.5%), as listed in **Table 3**.

The distribution of air in Comp\_LA is relatively homogeneous from the bottom to the top; however, the distribution of air is less homogeneous in either Comp\_MA or Comp\_SA. The difference in the air distribution in the composites may come from the preparation: as the size of aggregates reduces, it is harder for the epoxy to thoroughly cover every edge of an aggregate, especially in the closed small pores formed by two adjacent aggregates. Thus, there is a small peak in air percentage at the bottom of the Comp\_MA and Comp\_SA as presented in **Figures 4 (b)** and **(c)**. By scanning the composites by X-ray CT, we can not only have the global volumetric fractions of air, epoxy, and aggregates but also their local distributions in the composites, which can help us explain the difference in the dielectric constants of the composites in the following parts.

### Low frequency dielectric measurement by impedance analyzer

As mentioned before, ten discs of LA were tested by an impedance analyzer. The frequency-dependent dielectric permittivities are presented in **Figure 5**. As shown in **Figure 5**, the dielectric properties of the 10 LA discs are quite dispersive in the tested frequency range. It is known that the dielectric properties of a material are related to the polarizability ( $\alpha$ ) that depends on the charge displacement in a material. Each polarization mechanism describes the charge separation at different length scales: as the frequency increases, the dominant mechanism is as follows: (i) interfacial polarization from  $10^{-2} - 10^3$  Hz (also known as Maxwell-Wagner or space charge polarization), (ii) dipolar polarization from  $10^4 - 10^8$  Hz (also known as orientational polarization), (iii) atomic/ionic polarization and electronic polarization for frequencies larger than  $10^9$  Hz, respectively (Kasap 2007). In this test, the frequency range is from 1 Hz to 1 MHz where the interfacial and the dipolar polarizations are the main contributions. These two polarizations are strongly related to the mineralogical composition and the microstructure of a material. As shown by CT scanning, the aggregates in our study have different densities, and possibly various crystalline structures and orientations, which causes the variation in the dipolar polarization and the relaxation of space charges in the interfacial area. Thus, at low frequencies, a large variety in the dielectric properties of the 10 samples is observed, especially when the frequency is lower than 1000 Hz. However, the variety in dielectric permittivity is reduced when the frequency increases over  $10^5$  Hz since the relaxations cannot catch up with the high frequency. The frequency-dependent characteristic allows us to use the dielectric relaxation models to derive the dielectric constant at high frequencies.

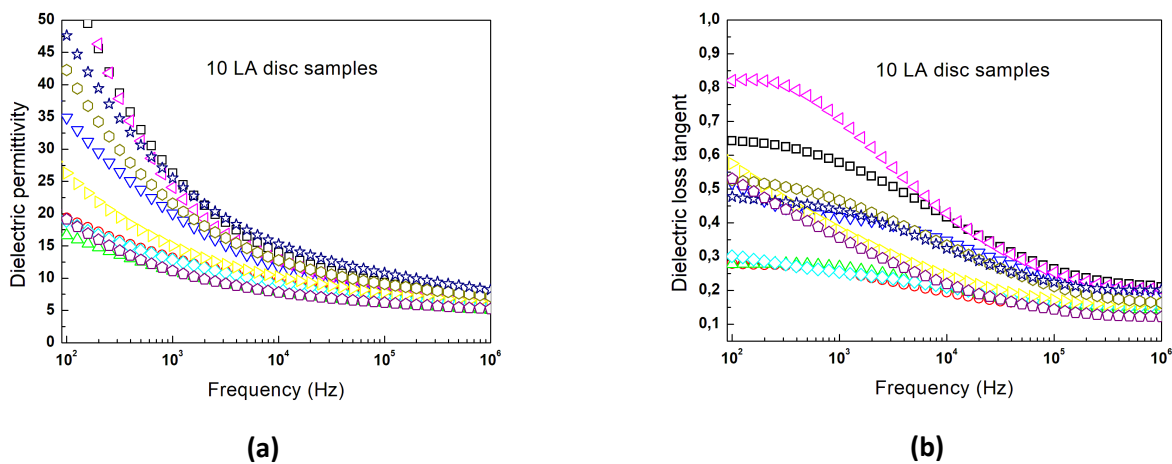


**Figure 5** Frequency-dependent dielectric properties of 10 LA discs **(a)** for the real permittivity and **(b)** for the dielectric loss tangent (The colors and symbols in the figures mean the ten pieces of LA discs.)

The real and imaginary parts of dielectric permittivity can be derived from the Kramers-Kronig relationships (Alvarez 1991):

$$\varepsilon'(\omega) = 1 + \frac{2}{\pi} \int_0^{+\infty} \frac{\omega' \varepsilon''(\omega')}{\omega'^2 - \omega^2} d\omega'$$

$$\varepsilon''(\omega) = -\frac{2\omega_r}{\pi} \int_0^{+\infty} \frac{1 - \varepsilon'(\omega')}{\omega'^2 - \omega_r^2} d\omega'$$

Several models have been developed based on this relationship, for example, Debye model and its derivatives such as Cole-Cole and Cole-Davidson models that have large applications in electrochemistry. In the case of construction materials, Jonscher universal dielectric response has been widely used to fit the dielectric properties by the electric susceptibility (Jonscher 1999, Bourdi et al. 2008, Ihamouten et al. 2018). To do the fitting by Jonscher model, the Origin non-linear curve fitting program has been used to optimize the parameters by multiple iterations.

$$\varepsilon_e(\omega) = \varepsilon_0 \chi_r \left( \frac{\omega}{\omega_r} \right)^{n-1} \left[ 1 - i \cot \left( \frac{n\pi}{2} \right) \right] + \varepsilon_\infty = \varepsilon_e' - i\varepsilon_e''$$

$$Re(\varepsilon_e(\omega)) = \varepsilon_e' = \varepsilon_0 \chi_r \left( \frac{\omega}{\omega_r} \right)^{n-1} + \varepsilon_\infty$$

$$Im(\varepsilon_e(\omega)) = \varepsilon_e'' = \varepsilon_0 \chi_r \left( \frac{\omega}{\omega_r} \right)^{n-1} \cot \left( \frac{n\pi}{2} \right)$$

where  $\varepsilon_0 = 8.854 \times 10^{-12}$  F/m is the permittivity of free space;  $\varepsilon_\infty$  (F/m) is the limiting high-frequency value of the real part of the effective permittivity.  $n$  is an empirical parameter without dimension that characterizes the charge in the amplitude as a function of frequency. Its value is usually between 0 and 1.  $\chi_r$  is the real part of the electric susceptibility to the frequency.  $\omega_r$  is a reference radial frequency for the fitting. The parameters used in the model are listed in **Table 4**. It can be found that the Jonscher model can be well fitted for all 10 samples with the correlation coefficient  $R^2$  approaching 1. This allows us to use the fitting parameters to derive the dielectric constant at higher frequencies that are not reached by the analyzer impedance. As mentioned before, the resonant frequency in the cavity is 540 MHz, then the dielectric constants at 540 MHz for the 10 LA discs are calculated, and the results are as listed in **Table 4**. The average dielectric constant of the 10 LA discs is about  $5.47 \pm 1.04$ . The result indicates a scatter of the dielectric constant for the 10 pieces of aggregates. Some empirical equations based on the relationship between the dielectric constant and density may help us estimate the dielectric constant of the aggregates [4, 18, 19] though they can hardly give an exact value. The calculated values based on three empirical equations have been listed in **Table 5**. Compared with the values deduced by Shutke, the average value of 5.5 fitted by the Jonscher model can be viewed as a reasonable reference for the LA samples. Although a simple average may be arbitrary and less representative of the whole aggregates, we must mention again that our primary interest in this part is to obtain the dielectric constant of the aggregates at high frequency that can be compared with the values calculated by mixing laws based on method 2 and method 3.

**Table 4** Parameters of the Jonscher model to derive the dielectric permittivity and the calculated relative dielectric permittivity at 0.54 GHz ( $R^2$  is a statistical measure that represents the proportion of the variance for a dependent variable that is explained by an independent variable or variables in a regression model. This value should approach 1).

LA disc	$\chi_r$	n	$\epsilon_\infty / \epsilon_0$	$R^2$	$\epsilon_{0.54\text{ GHz}} / \epsilon_0$
1	5.43	0.59	6.11	0.99991	6.19
2	4.47	0.76	4.77	0.99974	5.12
3	4.15	0.75	3.84	0.99988	4.11
4	5.94	0.70	4.04	0.99958	4.34
5	5.05	0.78	3.99	0.99996	4.47
6	7.98	0.50	6.72	0.99933	6.75
7	6.57	0.67	5.57	0.99937	5.58
8	8.17	0.63	6.19	0.99994	6.30
9	9.33	0.66	6.77	0.99984	6.96
10	7.48	0.66	4.80	0.99949	4.87

**Table 5** Dielectric constants calculated by the three empirical equations

	Ulaby: $\epsilon' = 1.96^p$	Shutke: $\epsilon' = (1+0.5p)^2$	Dobson: $\epsilon' = (1.01+0.44p)^2-0.062$
LA (2.712 g/cm <sup>3</sup> )	6.203	5.551	4.792
MA (2.701 g/cm <sup>3</sup> )	6.157	5.525	4.771
SA (2.697 g/cm <sup>3</sup> )	6.141	5.515	4.763

#### High frequency dielectric measurement by transmission resonant cavity

The dielectric constants of the samples in methods 2 and 3 at the resonance frequency of the cavity (540 MHz) are presented in **Figure 6**. It can be found that the dielectric constants of the samples, i.e., of the mixtures of aggregates and air, in the PTFE ring are lower than those of the composites, although the volumetric fractions of the aggregates are higher in the PTFE ring than those in the composites as shown in **Table 2** and **Table 3**. A possible reason could be the poor contact between the aggregates and the metal plate of the cavity. The texture of the aggregates as presented in **Figure 1** creates a layer of air between the aggregates and the metal plate, which creates a large interfacial resistance and reduces the tested values. Meanwhile, due to the unfixed surface, the contact depends on the fill state of the aggregates in the PTFE ring, which makes it necessary to repeat the measurement several times. However, in the case of the epoxy method, epoxy can well fix the

aggregates and the composites have a smooth surface, which increases the effective contact. Meanwhile, the dielectric constant of the epoxy is 2.73 at 540 MHz (measured by resonant cavity), which is closer to that of the aggregates than that of air. The reduced dielectric contrast in the composite will help to homogenize the mixed system. Hence, the measured dielectric constants of the composites are higher than those of the PTFE ring. In the next section, based on the obtained dielectric constants of the mixed systems (aggregates/air in method 2 and aggregates/epoxy/air in method 3), the mixing laws will be inversely used to calculate the dielectric constant of the aggregate phase.

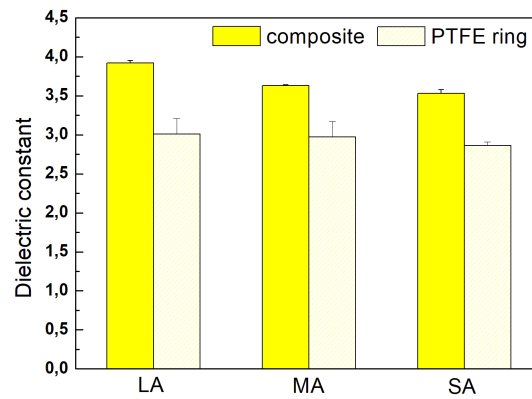


**Figure 6** Dielectric constants obtained by the transmission resonant cavity at 540 MHz

#### Application of mixing laws for calculating the dielectric constant of aggregates

Generally, the mixing laws are used to calculate the properties of a mixture based on the volumetric fraction of each phase and its physical parameter. In this study, an inverse calculation is conducted because the dielectric constants of the mixtures are accessible. It should be mentioned that in the mixtures of this work, each phase has a low electrical conductivity (aggregates:  $10^{-2}$ - $10^{-4}$  S/m (Araujo 2017), epoxy:  $\sim 10^{-9}$  S/m as presented in Figure S1). The difference between the dielectric constants (from 1 to 6) is not large enough to form a percolating structure. Thus, topological structures like the formation of connecting paths are not considered in this case. Table 6 indicates the mixing equations used in this study (Lichtenecker and Rother 1931, Looyenga 1965, Hickson et al. 2020). These equations can be divided into two groups based on their theoretical hypotheses: the matrix/inclusions group ((1)-(4)) and the statistical aggregate group ((5)-(8)). In the case of a PTFE ring, the mixing equations are used directly since there are only two phases: aggregates and air. In the case of the composite method, the group of matrix/inclusions ((1)-(4)) are used twice to treat the three-component system. A host phase is introduced to represent the matrix with two possibilities: (i) the host phase contains epoxy and aggregates, and the air is viewed as an inclusion phase; (ii) the host phase contains air and epoxy, and the aggregates are viewed as an inclusion phase. The calculation process for these two groups of mixing laws is presented in the supporting figures (Figures S2 - S5).

**Table 6** Two-phase analytical equations for the dielectric mixtures applied in this study (Lichtenecker and Rother 1931, Looyenga 1965, Hickson et al. 2020)

$\epsilon'_{r,eff}$  is the dielectric constant of the mixture;  $\epsilon'_{r,1}$  and  $\epsilon'_{r,2}$  are the dielectric constant of the first and the second phases.  $f$  is the volumetric fraction of the second phase in the mixture

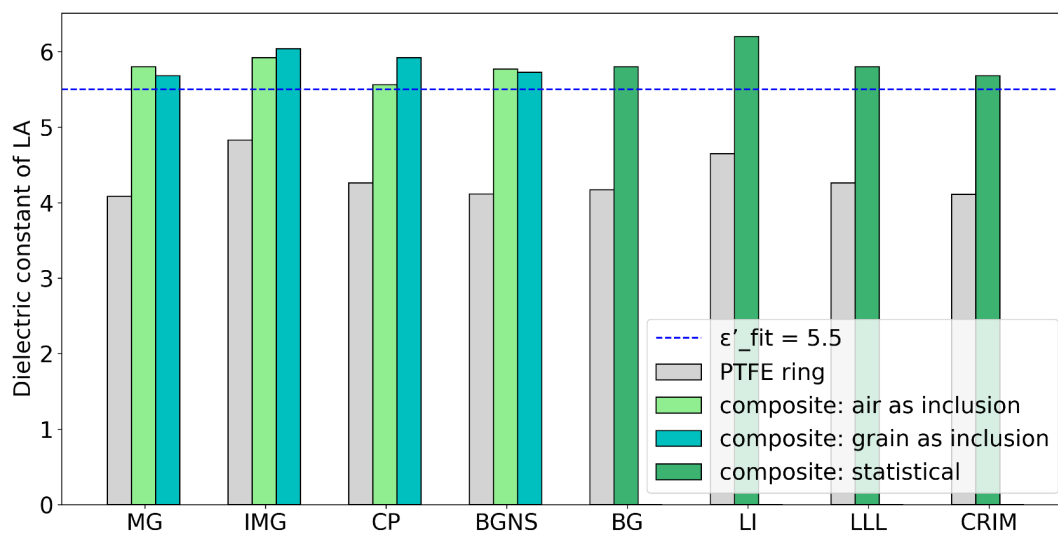
Name	Equation
------	----------

---

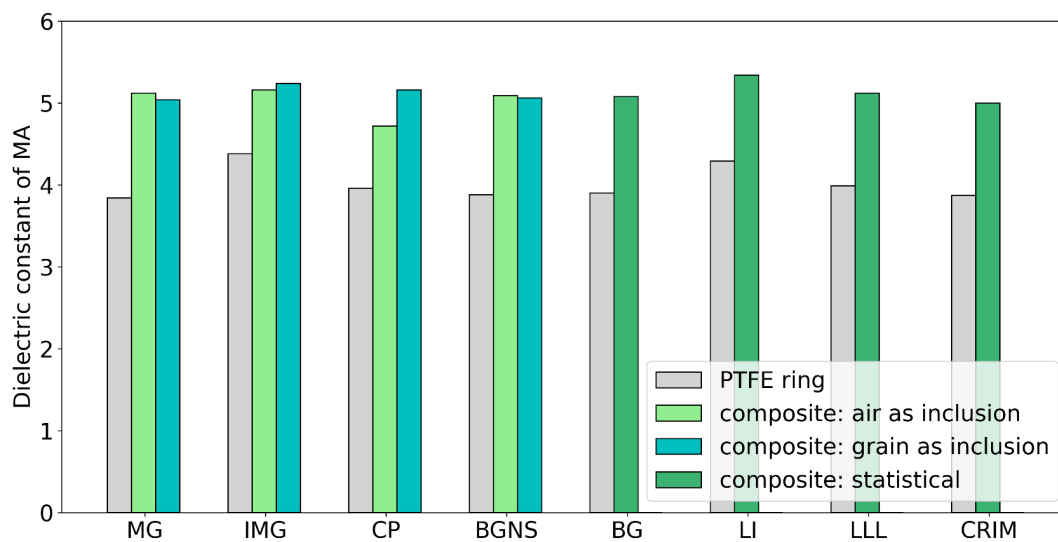
(1) Maxwell Garnett (MG)	$\epsilon'_{r,eff} = \epsilon'_{r,1} + 3f\epsilon'_{r,1} \frac{\epsilon'_{r,2} - \epsilon'_{r,1}}{\epsilon'_{r,2} + 2\epsilon'_{r,1} - f(\epsilon'_{r,2} - \epsilon'_{r,1})}$
(2) Inverse Maxwell Garnett (IMG)	$\epsilon'_{r,eff} = \epsilon'_{r,2} + 3(1-f)\epsilon'_{r,2} \frac{\epsilon'_{r,1} - \epsilon'_{r,2}}{\epsilon'_{r,1} + 2\epsilon'_{r,2} - (1-f)(\epsilon'_{r,1} - \epsilon'_{r,2})}$
(3) Coherent Potential (CP)	$\epsilon'_{r,eff} = \epsilon'_{r,1} + f(\epsilon'_{r,2} - \epsilon'_{r,1}) \frac{3\epsilon'_{r,eff}}{3\epsilon'_{r,eff} + (1-f)(\epsilon'_{r,2} - \epsilon'_{r,1})}$
(4) Bruggeman nonsymmetric (BGNS)	$\frac{\epsilon'_{r,2} - \epsilon'_{r,eff}}{\epsilon'_{r,2} - \epsilon'_{r,1}} = (1-f) \left( \frac{\epsilon'_{r,eff}}{\epsilon'_{r,2}} \right)^{\frac{1}{3}}$
(5) Bruggeman (BG)	$(1-f) \frac{\epsilon'_{r,1} - \epsilon'_{r,eff}}{\epsilon'_{r,1} + 2\epsilon'_{r,eff}} + f \frac{\epsilon'_{r,2} - \epsilon'_{r,eff}}{\epsilon'_{r,2} + 2\epsilon'_{r,eff}} = 0$
(6) Lichtenecker (LI)	$\log \epsilon'_{r,eff} = (1-f) \log \epsilon'_{r,1} + f \log \epsilon'_{r,2}$
(7) Looyenga-Landau-Lifshitz (LLL)	$\epsilon'_{r,eff}{}^{\frac{1}{3}} = (1-f) \epsilon'_{r,1}{}^{\frac{1}{3}} + f \epsilon'_{r,2}{}^{\frac{1}{3}}$
(8) Complex Refractive Index Model (CRIM)	$\sqrt{\epsilon'_{r,eff}} = (1-f) \sqrt{\epsilon'_{r,1}} + f \sqrt{\epsilon'_{r,2}}$

---

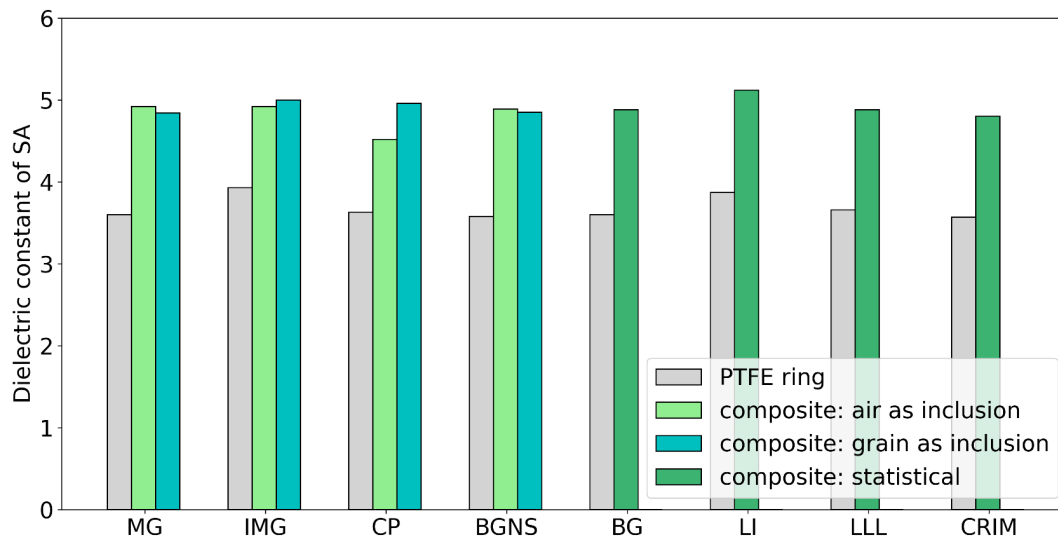
The results for the aggregates calculated by the analytical approaches for the dielectric mixture systems from the two methods are presented in **Figure 7**. On one hand, it can be found that the results calculated by the PTFE ring (method 2) in gray are always lower than those calculated by the composite (method 3). Considering the values fitted by the Jonscher model in the case of LA presented in **Figure 7 (a)**, it can be found that the result of LA calculated by the composite is closer than that by the conventional PTFE ring. As mentioned before, the analytical approaches are adapted to diluted systems where the volumetric fraction of one phase should be much smaller than that of the other phase (Asami K. (2002)). In the case of method 2, as listed in **Table 2**, the volumetric fraction of air in the PTFE ring is too high (over 20%) to meet the assumption. However, in the case of composite, the presence of epoxy can effectively reduce the air volumetric fraction (about 2.5%). Thus, adding epoxy can be viewed as a homogenization process that favors an effective medium approximation. On the other hand, if comparing the results by the composite method, it can be found that the selection of the inclusion phase for the matrix/inclusions group does not obviously change the dielectric constant of the aggregates. Moreover, the results calculated by the matrix/inclusions group and statistical group are also very close. If using the value of 5.5 for LA as a reference, the values calculated by CP (inclusion of air) and CRIM seem better than those obtained by the other mixing laws, but considering that 5.5 is the average value of 10 LA discs with an inhomogeneous microstructure, the difference in the calculations by the mixing laws can be considered as negligible.



(a)



(b)



(c)

**Figure 7** Application of mixing laws in Table 6 to calculate the dielectric constant of LA (a), MA (b) and SA (c) (Maxwell Garnett (MG), Inverse Maxwell Garnett (IMG), Coherent Potential (CP), Bruggeman (nonsymmetric) (BGNS), Bruggeman Symmetric (BG), Lichtenecker (LI), Looyenga-Landau-Lifshitz (LLL) and Complex Refractive Index Model (CRIM))

Additionally, if we come back to the difference in the dielectric constants for aggregates with different size distributions as illustrated in Figure 7 (a) to (c), it can be found that the dielectric constants of LA in both methods 2 and 3 are the highest, those for MA are intermediate, and those for SA are the lowest, which agrees with the results by the density empirical equations in **Table 5**. The size-dependent effect on the dielectric constant of the aggregates may result from several possibilities: firstly, from the point of view of microstructure, although the aggregates come from the same provider, the cutting process may destroy the orientation plane of the rocks and simultaneously create defects. This process may reduce the dielectric constant of MA and SA. Secondly, from the point of view of preparation, as mentioned in the CT analysis, many small bubbles have been found in the interfacial regions of epoxy/ aggregates in Comp\_MA and Comp\_SA. These air bubbles were introduced during the preparation. Although the global air volumetric fractions are similar in the three composites, the distribution of the air is different, which reduces the dielectric constant of Comp\_MA and Comp\_SA, and consequently affects the calculation for SA and MA by mixing laws. The phenomenon that the dielectric permittivity of matrix-inclusion composite shows a sensitive dependence on the grain size distribution has been reported by Spanoudaki and Pelster 2001, and Matous et al. 2017, but it must be mentioned that the assumption of spheres with polydispersity is not suitable for the aggregate case. Meanwhile, the difference between SA and LA from the mixing laws calculation is around 1 which is in the deviation of the low-frequency measurement by method 1. Hence, the size dependence of the dielectric constant at microwave frequency will not be overemphasized in this study, but we will study it by using rock samples with mono-mineralogy in the future.

## Conclusions

In this work, we provide a novel epoxy-based composite method to estimate the dielectric constant of aggregates with different size distributions for the interpretation of GPR. Compared with the common binders in the construction materials like cement or bitumen, the preparation of the sample based on epoxy is simple and water-free which avoids humidity influence on the dielectric properties. Meanwhile, the epoxy composites are stable at room temperature without deformation, which allows us to do the morphology analysis. Compared with a conventional method (measuring aggregates directly in a PTFE ring), the epoxy composite can give more reliable values, which agree with the average value fitted by the Jonscher model and the empirical equation based on density. Two possible reasons can explain this better performance: (1) a smooth surface of the composite and a high adherence between epoxy and aggregates can ensure effective contact between samples and the metal plate of the cavity. (2) the use of epoxy largely reduces the air volumetric fraction, which makes the composite closer to a diluted system which can be closer to the hypothesis of analytical approaches for dielectric mixtures based on mean-field theories.

## Acknowledgment

This work has been financially supported by the French Agence Nationale de la Recherche through the "Investissements d'avenir" program (ANR-10- EQPX-37 MATMECA Grant) and French "Carnot Clim'adapt 2022". The authors are grateful to AGIR-CTCV for providing the aggregates with different size distributions. The authors are also grateful to Mr. Bruno Beaucamp and Mr. Cyril Ledun for the dielectric cavity measurement.

## Reference

- AL-Qadi I.L., Lahouar S. (2005) Measuring layer thicknesses with GPR- Theory to practice. *Constr Build Mater.* 19: 763-772. doi: 10.1016/j.conbuildmat.2005.06.005
- Adous M., Queffelec P., Laguerre L. (2006) Coaxial/cylindrical transition line for broadband permittivity measurement of civil engineering materials. *Meas Sci Technol.* 17: 2241. doi: 10.1088/0957-0233/17/8/026
- Alvarez F., Alegria A., Colmenero J. (1991) Relationship between the time domain Kohlrausch-Williams-Watts and frequency-domain Havriliak-Negami relaxation function. *Phys Rev B Condens Matter.* 7306. doi: 10.1103/PhysRevB.44.7306
- Andrade C., Blanco V.M., Collazo A., Keddami M., Noavo X.R., Takenouti H. (1999) Cement paste hardening process studied by impedance spectroscopy. *Electrochim. Acta* 44: 4313-4318. doi: 10.1016/S0013-4686(99)00147-4
- Araujo S., Beaucamp B., Delbreilh L., Dargent E., Fauchard C. (2017) Compactness/density assessment of newly paved highway containing recycled asphalt pavement by means of non-nuclear method. *Constr Build Mater.* 154: 1151-1163. doi: 10.1016/j.conbuildmat.2017.07.075
- Araujo S. (2017) Compactness assessment of asphalt pavement and wideband characterization of rocks dielectric properties. PhD thesis. 2017. Université de Rouen Normandie
- Asami K. (2002) Characterization of heterogeneous systems by dielectric spectroscopy. *Prog Polym Sci.* 27: 1617-1659. doi: 10.1016/S0079-6700(02)00015-1
- Ayoub M. W. B. (2018) Measurement devices of dielectric constants in wet materials: towards a better traceability of the measurement of the moisture in solids. PhD thesis. Université d'Aix-Marseille
- Benedetto A., Fabio T., Ciampoli L. B. D'Amico F., (2016) An overview of ground-penetrating radar signal processing techniques for road inspections. *Signal Processing*, 132: 201-209. doi: 10.1016/j.sigpro.2016.05.016
- Bourdi T., Rhazi J. E., Boone F., Ballivy G. (2008) Application of Jonscher model for the characterization of the dielectric permittivity of concrete. *J Phys D Appl Phys.* 41: 205410. doi: 10.1088/0022-3727/41/20/205410

- Chen L. F., Ong C. K., Neo C.P., Varadan V. V., Varadan V. K. (2004) Microwave electronics measurement and materials characterization. John Wiley & Sons. Ltd. Chapter 2
- Dérobot X., Fauchard C., Côte P., Le Brusq E., Guillanton E., Dauvignac J., Pichot C. (2001) Step-frequency radar applied on thin road layers. *J Appl Geophys.* 47: 317-325. doi: 10.1016/S0926-9851(01)00075-1
- Dobson M.C., Ulaby F.T., Hallikainen M.T., El-Rayes M.A. (1985) Microwave dielectric behavior of wet soil - Part II: Dielectric mixing models. *IEEE Trans Geosci Remote Sens.* 23: 35-46. doi: 10.1109/TGRS.1985.289498
- Fan B., He D., Liu Y. Bai J. (2017) Influence of Thermal Treatments on the Evolution of Conductive Paths in Carbon Nanotube-Al<sub>2</sub>O<sub>3</sub> Hybrid Reinforced Epoxy Composites. *Langmuir* 33: 9680–9686. doi: 10.1021/acs.langmuir.6b03915
- Fauchard C., Li B., Laguerre L., Héritier B., Benjelloun N., Kadi M. (2013) Determination of the compaction of hot mix asphalt using high-frequency electromagnetic methods. *NDT E Int.* 60: 40-51. doi: 10.1016/j.ndteint.2013.07.004
- Hickson D.C., Boivin A.L., Tsai C.A., Daly M.G., Ghent R.R. (2020) Modeling the dielectric properties of minerals from crystals to bulk powers for improved interpretation of asteroid radar observations. *J Geophys Res Planets.* 125. 7. doi: 10.1029/2019JE006141
- Ihamouten A., Bosc F., Guan B., Le Bastard C., Fauchard C., Lambot S., Derobert X. (2018) Full-waveform inversion using a stepped-frequency GPR to characterize the tack coat in hot-mix asphalt (HMA) layers of flexible pavements, *NDT E Int.* 95: 17-25. doi: 10.1016/j.ndteint.2017.12.006
- Jonscher A. K. (1999) Dielectric relaxation in solids. *J Phys D Appl Phys.* 32 R57. doi: 10.1088/0022-3727/32/14/201
- Kaatze U. (2013) Measuring the dielectric properties of materials. Ninety-year development from low-frequency techniques to broadband spectroscopy and high-frequency imaging. *Meas Sci Technol.* 24. 012005. doi: 10.1088/0957-0233/24/1/012005
- Kasap S.O. (2007) Principles of electronic materials and devices. New York: McGraw Hill Education. p. 583-609
- Lai W.W.L., Dérobot X., Annan A.P. (2018) A review of Ground Penetrating Radar application in civil engineering: A 30-year journey from Locating and Testing to Imaging and Diagnosis. *NDT E Int.* 96:58–78. doi: 10.1016/j.ndteint.2017.04.002
- Li Z. S., Tang L. S. (2019) Using synchrotron-based X-ray microcomputed tomography to characterize water distribution in compacted soils. *Adv Mater Sci Eng.* 7147283. doi: 10.1155/2019/7147283
- Lichtenecker K. and Rother K. (1931) Die Herleitung des logarithmischen Mischungsgesetzes aus allgemeinen Prinzipien der Stationären Stromung. *Phys. Z* 32: 255-260
- Looyenga H. (1965) Dielectric constants of heterogeneous mixture. *Physica* 31: 401-406. doi: 10.1016/0031-8914(65)90045-5
- Matous K., Geers M. G. D., Kouznetsova V. G., Gillman A. (2017) A review of predictive nonlinear theories for multiscale modeling of heterogeneous materials. *J Comput Phys.* 330: 192-220. doi: 10.1016/j.jcp.2016.10.070
- Robert A. (1998) Dielectric permittivity of concrete between 50 MHz and 1 GHz and GPR measurements for building materials evaluation. *J Appl Geophys.* 40: 89-194. doi: 10.1016/S0926-9851(98)00009-3
- Robinson D.A. and Friedman S.P. (2003) A method for measuring the solid particle permittivity or electrical conductivity of rocks, sediments and granular materials. *J Geophys Res.* 108 B2. doi: 10.1029/2001JB000691
- Saba S., Delage P., Lenoir N., Cui Y. J., Tang A. M., Barnichon J. D. (2014) Further insight into the microstructure of compacted bentonite–sand mixture. *Eng Geol.* 168: 141-148. doi: 10.1016/j.enggeo.2013.11.007
- Sihvola A., Kong J.A. (1988) Effective permittivity of dielectric mixture. *IEEE Trans Geosci Remote Sens.* 26: 420-429. doi: 10.1109/36.3045
- Smith I.B., Lalick D.E., Rezza C., Horgan B.H.N., Whitten J.L., Nerozzi S., Holt J.W. (2021) A solid interpretation of

bright radar reflectors under the Mars south polar ice. *Geophys Res Lett.* 48. 5. doi: 10.1029/2021GL093618

Spanoudaki A., Pelster R. (2001) Effective dielectric properties of composites materials: The dependence on the particle size distribution, *Phys Rev B Condens Matter.* 64: 064205. doi: 10.1103/PhysRevB.64.064205

Tuncer E., Serdyuk Y.V., Gubanski S.M. (2002) Dielectric mixtures – electrical properties and modeling. *IEEE Trans Dielectr Electr Insul.* 9: 809-828. doi: 10.1109/TDEI.2002.1038664

Ulaby F.T., Bengal T.H., Dobson M.C., East J.R., Garvin J.B., Evans D.L. Microwave dielectric properties of dry rocks, *IEEE Trans Geosci Remote Sens.* 28: 325-336. doi: 10.1109/36.54359

Ulrich T. J., McCall K. R., Guyer R. A. (2002) Determination of elastic moduli of rock samples using resonant ultrasound spectroscopy. *J Acoust Soc Am.* 111:1167. doi: 10.1121/1.1463447

Wagner N., Bore T., Robinet J.C., Coelho D., Taillade F., Delepine-Lesoille S. (2013) Dielectric relaxation behavior of callovo-oxfordian clay rock: a hydraulic-mechanical-electromagnetic coupling approach. *J Geophys Res Solid Earth.* 118: 4729-4744. doi: 10.1002/jgrb.50343

Zheng Y. L., Zhao X. B., Zhao Q.H., Li J. C., Zhang Q. B. (2020) Dielectric properties of hard rock minerals and implications for microwave-assisted rock fracturing. *Geomech Geophys Geo-Energy Geo-Resour.* 6. doi: 10.1007/s40948-020-00147-z

Standard Test Method for Density and Relative Density (Specific Gravity) of Liquids by Bingham Pycnometer, ASTM D1217-20

Ametek Solartron Analytical ModuLab XM user guide Manual:  
<https://www.ameteksi.com/support-center/solartron-analytical/product-manuals>

## Supporting figures:

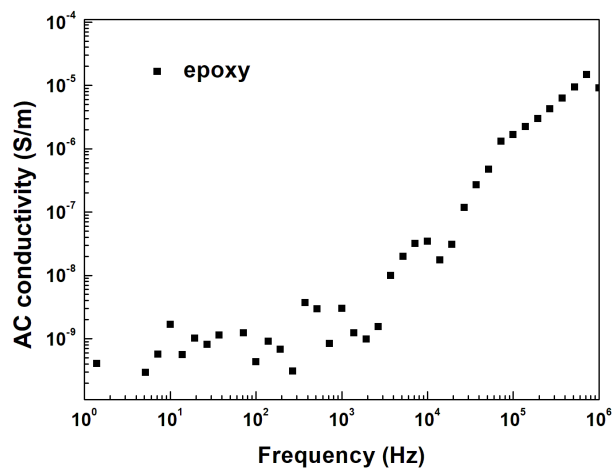
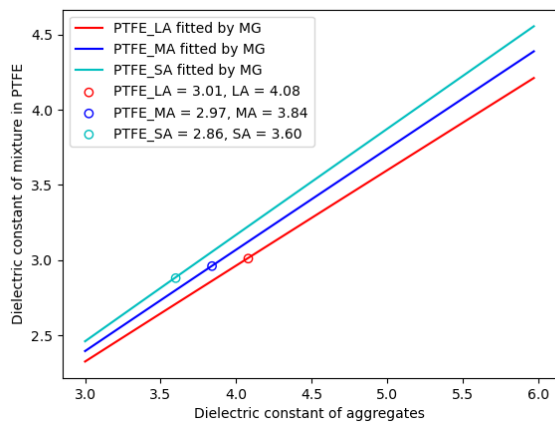
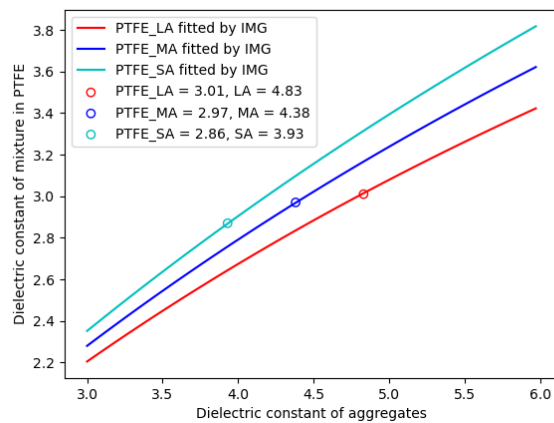


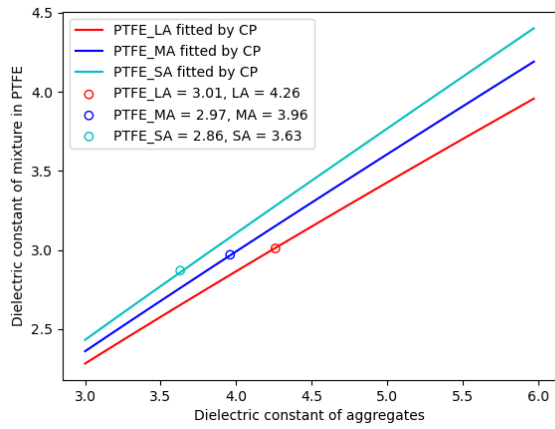
Figure S1 Ac conductivity of epoxy from 1 to 1 MHz



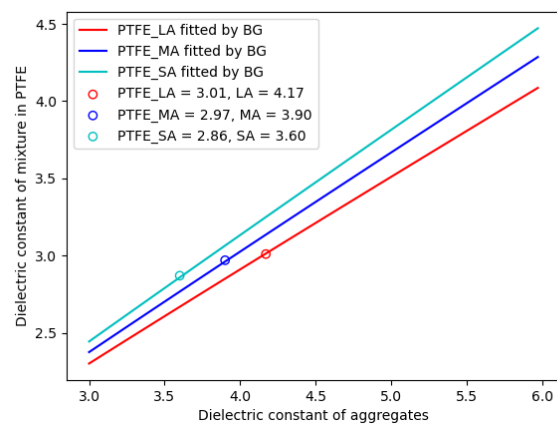
(a)



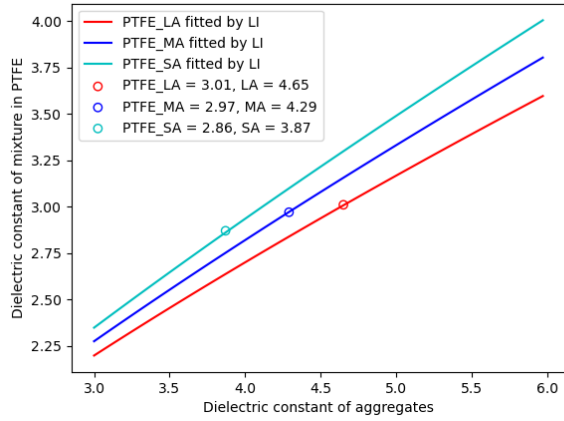
(b)



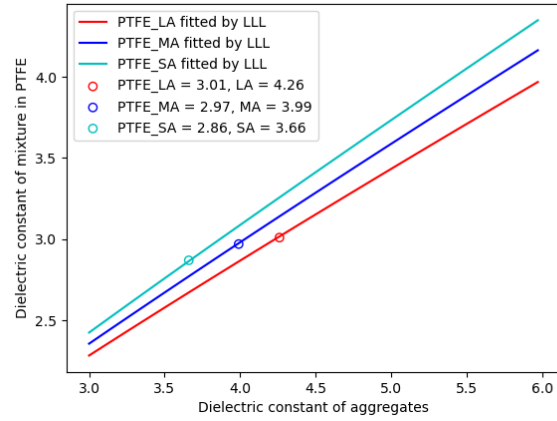
(c)



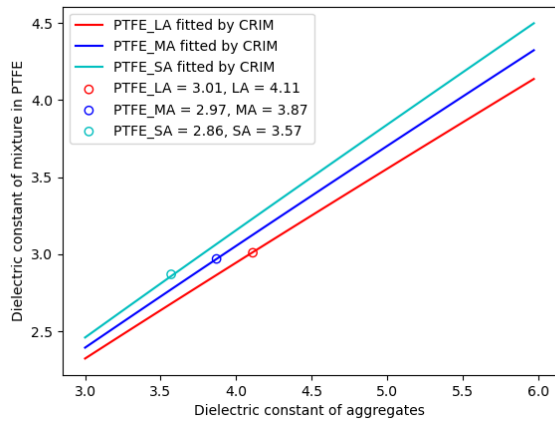
(d)



(e)



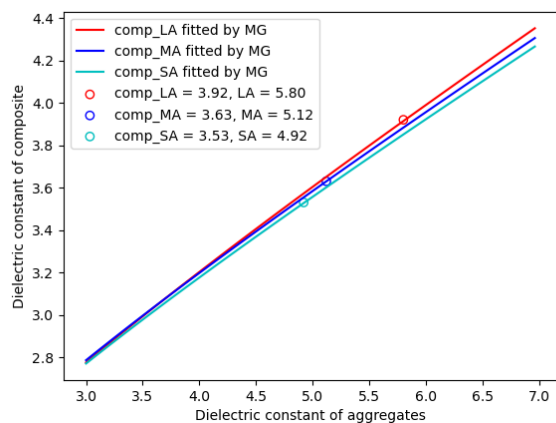
(f)



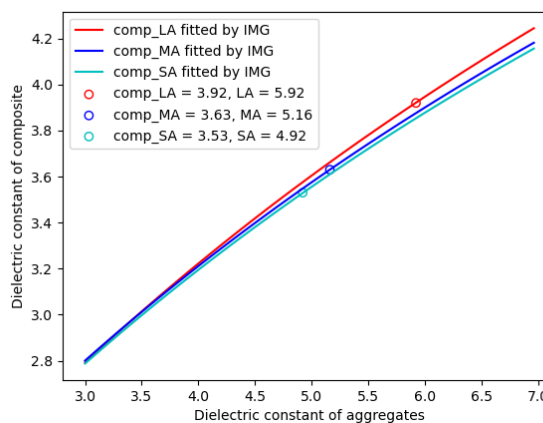
(g)

**Figure S2** Calculating the dielectric constants of aggregates by mixing laws in Table 6 based on method 2 PTFE

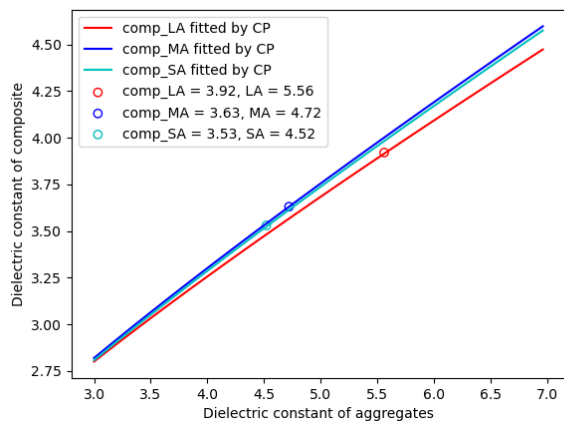
ring: **(a)** Maxwell Garnett (MG), **(b)** Inverse Maxwell Garnett (IMG), **(c)** Coherent Potential (CP), **(d)** Bruggeman Symmetric (BG), **(e)** Lichtenecker (LI), **(f)** Looyenga-Landau-Lifshitz (LLL) and **(g)** Complex Refractive Index Model (CRIM)



**(a)**

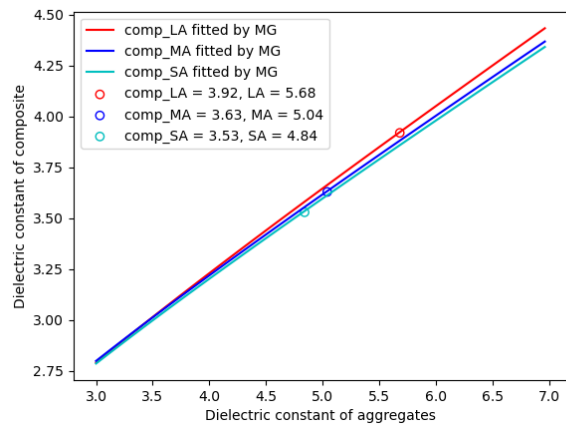


**(b)**

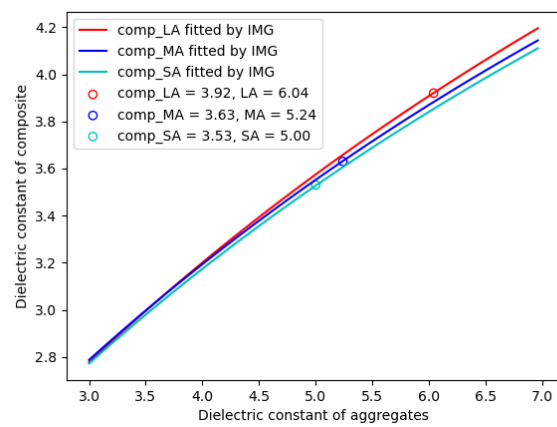


**(c)**

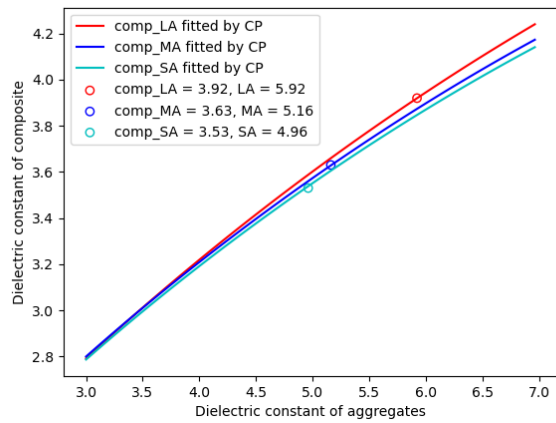
**Figure S3** Calculating the dielectric constants of aggregates by matrix/inclusion mixing laws where inclusion is air in Table 6 based on method 3: **(a)** Maxwell Garnett (MG), **(b)** Inverse Maxwell Garnett (IMG), **(c)** Coherent Potential (CP)



(a)

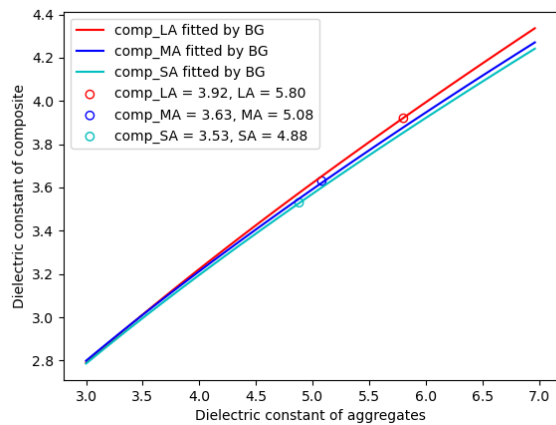


(b)

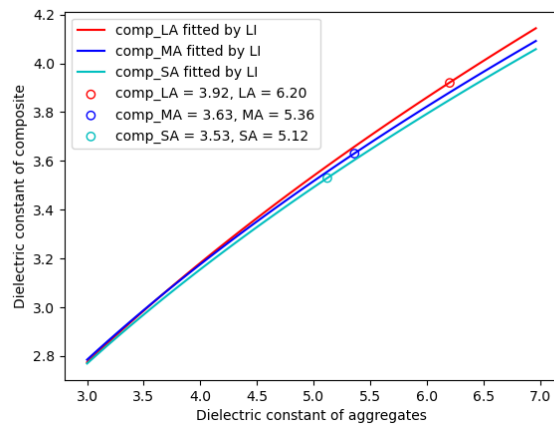


(c)

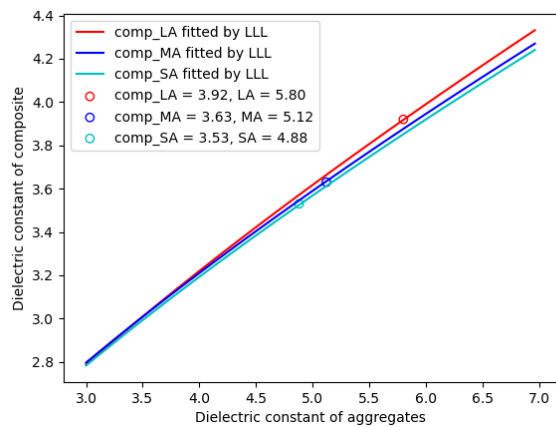
**Figure S4** Calculating the dielectric constants of aggregates by matrix/inclusion mixing laws where inclusion is aggregates in Table 6 based on method 3: **(a)** Maxwell Garnett (MG), **(b)** Inverse Maxwell Garnett (IMG), **(c)** Coherent Potential (CP)



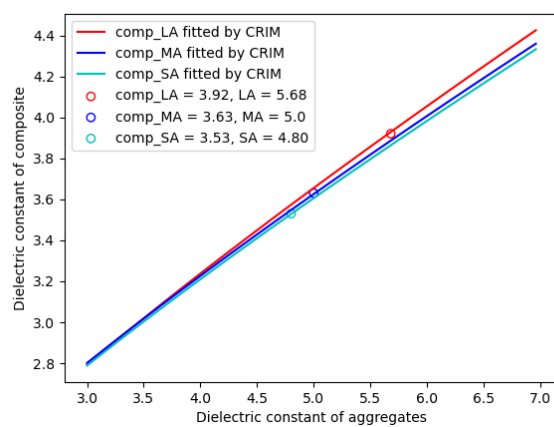
(a)



(b)



(c)



(d)

**Figure S5** Calculating the dielectric constants of aggregates by statistical mixing laws in Table 6 based on method 3: **(a)** Bruggeman Symmetric (BG), **(b)** Lichtenecker (LI), **(c)** Looyenga-Landau-Lifshitz (LLL) and **(d)** Complex Refractive Index Model (CRIM)